Axisymmetric motion of capsules through cylindrical channels

By CHRISTOPHE QUÉGUINER
AND DOMINIQUE BARTHÈS-BIESEL

Université de Technologie de Compiègne, UMR CNRS 6600, B.P. 20529,
60 205 Compiègne Cedex, France

A boundary integral method is used to model the flow of capsules into pores. An axisymmetric configuration is considered where the capsule and the pore axis coincide. The channel is a cylinder with hyperbolic entrance and exit regions. The capsule has a discoidal unstressed shape, is filled with a Newtonian liquid and is enclosed by a very thin membrane with various elastic properties (neo-Hookean or area-incompressible). The motion of the internal capsule liquid and of the suspending fluid is governed by the Stokes equations whose solution is expressed as boundary integrals. Those are computed by a collocation technique, where points are distributed on the capsule interface, on the channel walls and on the entrance and exit sections of the flow domain. The capsule interface mechanics follow the theory of large deformations of elastic membranes. The numerical model uses a forward time-stepping method, where the position and the deformation of the capsule are computed at each time step.

The model allows the study of the effect of a number of parameters (capsule size and geometry, membrane elastic properties) on the flow. The entrance length in the pore, the steady additional pressure drop at equilibrium and the capsule deformed profiles are determined. It is found that the entrance of a capsule into a pore is not sensitive to downstream conditions; but the length of tube necessary to reach steady conditions depends strongly on capsule size and membrane behaviour. Bursting of capsules with a neo-Hookean membrane is predicted to occur through a phenomenon of continuous elongation. The flow of a capsule with a membrane that resists area dilatation depends strongly on particle size and shape.

1. Introduction

Capsules are composite particles consisting of a liquid internal medium, enclosed by a very thin deformable membrane. This definition covers a large number of particles ranging from liquid droplets, to biological cells (red blood cells for example), and to artificial capsules. Blood cells have been extensively studied, both experimentally and theoretically for obvious physiological reasons. The interest in artificial capsules is more recent. Indeed, artificial capsules occur in many practical applications in cosmetic, pharmaceutical or agricultural industries. They are presently being considered in medical applications, for the encapsulation of organ cells before implantation.

When suspended in another liquid subjected to flow, a capsule deforms. However, the prediction of the corresponding motion is a difficult problem of continuum mechanics, because fluid mechanics (internal and external liquid motion) and solid

mechanics (deformation of the membrane) are strongly coupled. The case of capsules (or cells) suspended in unbounded shear flows is well documented both on the experimental and theoretical side. Experimental studies of red blood cells in simple shear flow have shown that the cells deform and orient with respect to streamlines, while the membrane rotates around the steady deformed shape (Fischer, Stohr & Schmid-Schönbein 1978, Sutera, Pierre & Zahalak 1989). Recent experimental results on artificial capsules in shear flows confirm this behaviour (Chang & Olbricht 1993*a, b*; Burger & Rehage 1992). On the theoretical side, models of the motion of initially spherical cells in shear flow have been proposed for the case where the cell deformation is small (Barthès-Biesel 1991). The case of cells deformed into an assumed ellipsoidal shape has also been solved (Keller & Skalak 1982; Sutera *et al.* 1989) and used to interpret experimental observations of red blood cells in shear flows. Numerical studies of the large deformations of capsules are now available, in pure straining flow (Li, Barthès-Biesel & Helmy 1988, Pozrikidis; 1990) or in simple shear flow (Pozrikidis 1995; Zhou & Pozrikidis 1995).

A case of interest that has been only scantily addressed pertains to the flow of capsules in cylindrical tubes. This situation is encountered during filtration processes where a capsule suspension is forced through a filter with small pores. On the physiological side, this flow occurs in the microcirculation, where 8 μm discoidal red blood cells squeeze into capillary vessels with a diameter as small as 4 μm. Owing to the complexity of the mechanical processes that occur during filtration or microcirculation, it is difficult to distinguish among the roles of the various physical parameters: flow strength, size ratio between the tube and the cell, initial cell geometry, membrane mechanical properties, internal viscosity. Consequently, filtration experiments are difficult to interpret other than in a qualitative sense. Similarly, from the physiological point of view, it is difficult to determine which of those parameters affect the flow in the microcirculation most.

Some theoretical models of the motion of red blood cells in capillary tubes have been proposed over the years. The cell is then represented as a capsule with an area-incompressible membrane. This limits strongly the possible deformations of the interface. When the liquid film between the cell and the wall is small enough, it is possible to use the lubrication approximation. This approach was taken by Secomb *et al.* (1986) for steady axisymmetric situations where the cell and the tube are coaxial. The solution of the lubrication problem is obtained in the case of an area incompressible membrane, with negligible shear resistance. The problem is then amenable to a composite analytical/numerical solution. When shear elasticity and bending resistance are included, a numerical model must be developed. In this case, the stress-free reference state of the membrane is assumed to be spherical (this obviously means that there is a volume difference between the reference and deformed states). Flared cell shapes analogous to those observed in human microcirculation are then predicted. The case of very narrow tubes (with a diameter slightly above the minimal value necessary for a cell to flow while keeping its surface and volume constant) has been studied by Halpern & Secomb (1989). They predict that the cell takes on a slug shape with either convex or concave rear ends depending on the size ratio between the cell and the tube. Hsu & Secomb (1989) have also considered three-dimensional situations where the cell is off-centre, but find only a small additional hydrodynamic perturbation due to non-axisymmetry. This result justifies the use of axisymmetric models.

The objective of this paper is to investigate the hydrodynamics of a capsule in tube flow. We first study spherical capsules with a neo-Hookean membrane. This

corresponds to artificial capsules with a cross-linked polymer membrane (nylon, polylysine, etc.), such as those commonly used in practical applications. Then discoidal capsules are considered, with an elastic membrane that strongly opposes area dilatation. This corresponds to cells surrounded by a bilayer type of membrane (e.g. red blood cells). Rather than seeking only steady states, the full entrance process into the tube is modelled and the motion of the particle inside the cylindrical tube is followed until a steady state is reached. This procedure has two advantages. First, monitoring the capsule motion into the tube yields the mapping between the positions of the membrane material points in the reference and deformed states. Secondly, it gives information regarding the transient phenomena during entrance and thus helps understand some filtration experiments where such transients are specifically recorded (Fisher, Wenby & Meiselman 1992). In particular, the length of tube necessary to reach a steady state is at present unknown. A similar fully unsteady situation was considered recently by Leyrat-Maurin & Barthès-Biesel (1994, referred to as I in the following) who modelled the flow of initially spherical capsules through hyperbolic pores. It will be of interest to compare the predictions of the two models, particularly during the entrance process. As regards the steady-state situation, the equilibrium shape of the capsule is also unknown. It will be seen that this shape depends in a complex fashion on the capsule properties and on the flow strength.

The model is based on the boundary integral formulation of the Stokes equations (Ladyzhenskaya 1969). The numerical procedure follows that of Leyrat-Maurin & Barthès-Biesel (1994) for the flow of a capsule in a hyperbolic constriction. The problem statement is presented in §2 together with the governing equations. The numerical method and the validation procedure are discussed in §3. Typical results obtained for capsules with a neo-Hookean membrane, that are either smaller or larger than the tube, are presented in detail in §§4 and 5. Capsules with a membrane that opposes area dilatation are considered in §6, and the effect of particle size and shape is discussed.

2. Problem statement

The pore is an axisymmetric channel consisting of a cylindrical tube of radius r_t and length $L_t r_t$, with symmetrical coaxial hyperboloidal entrance and exit sections. A set of cylindrical coordinates (x, r, ϕ) is used with origin O at the cylindrical tube entrance (figure 1). The equation of the channel wall (x_B, r_B) is

$$r_B^2 - x_B^2 (1 - \zeta_0^2)/\zeta_0^2 = 1 \quad \text{for} \quad x_B \leqslant 0, \tag{2.1a}$$

$$r_B^2 = 1 \quad \text{for} \quad 0 \leqslant x_B \leqslant L_t, \tag{2.1b}$$

$$r_B^2 - (x_B - L_t)^2 (1 - \zeta_0^2)/\zeta_0^2 = 1 \quad \text{for} \quad x_B \geqslant L_t, \tag{2.1c}$$

where lengths have been scaled by r_t. The parameter ζ_0 is the cosine of the angle of the hyperbola asymptotes with the x-axis, and thus the smaller ζ_0, the sharper the entrance of the pore. The pore is filled with a Newtonian incompressible fluid with viscosity μ, flowing with a constant flow rate Q. In the absence of any particle, the velocity and pressure fields in the channel are denoted $\boldsymbol{v}^\infty$ and P^∞.

The capsule consists of a drop of a Newtonian incompressible fluid with viscosity $\lambda\mu$ surrounded by an infinitely thin membrane with negligible bending resistance and with a surface elastic Young modulus E_s. In its stress-free state, the capsule has a discoidal shape with radius Rr_t and thickness $2Dr_t$. The revolution axis of
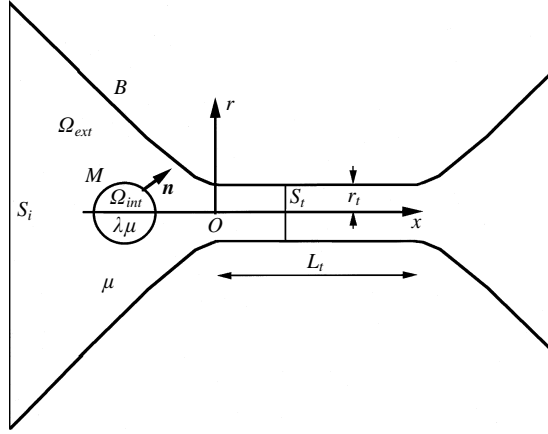
FIGURE 1. Schematic of the problem.

the particle is aligned with the tube axis. The situation is thus fully axisymmetric. Furthermore, the tube is sufficiently long for the capsule to reach a steady motion. Consequently, entrance and exit processes are decoupled and may be treated independently.

Non-dimensional quantities are used throughout, based on the following scales: r_t for lengths, E_s for elastic tensions, V_0 (the mean tube velocity, $V_0 = Q/\pi r_t^2$) for velocities, $\mu V_0/r_t$ for viscous stresses and pressures.

2.1. *Equations of motion for the fluids*

The domains occupied by the internal and external liquids are denoted as Ω_{int} and Ω_{ext}. For the entrance process, the suspending fluid domain Ω_{ext} is bounded by the capsule membrane (M), the channel walls (B) and by two sections S_i and S_t located respectively in the entrance funnel and in the cylindrical part of the pore. For the exit process, Ω_{ext} is bounded by M, B, S_t and a section S_o located in the exit funnel. Normal unit vectors $\boldsymbol{n}$ are pointing into Ω_{ext}. Under the assumption that the particle Reynolds number is very small, the velocity and pressure in the internal and external fluids satisfy the Stokes equations:

$$\nabla \cdot \boldsymbol{\sigma}^{int} = \boldsymbol{0}, \quad \nabla \cdot \boldsymbol{v}^{int} = 0 \quad \text{in} \quad \Omega_{int}, \tag{2.2a}$$

$$\nabla \cdot \boldsymbol{\sigma}^{ext} = \boldsymbol{0}, \quad \nabla \cdot \boldsymbol{v}^{ext} = 0 \quad \text{in} \quad \Omega_{ext}, \tag{2.2b}$$

with

$$\boldsymbol{\sigma}^{int} = -P^{int}\boldsymbol{I} + \lambda(\nabla\boldsymbol{v}^{int} +^T \nabla\boldsymbol{v}^{int}) \quad \text{in} \quad \Omega_{int},$$

$$\boldsymbol{\sigma}^{ext} = -P^{ext}\boldsymbol{I} + (\nabla\boldsymbol{v}^{ext} +^T \nabla\boldsymbol{v}^{ext}) \quad \text{in} \quad \Omega_{ext},$$

where $\boldsymbol{\sigma}^{ext}$ and $\boldsymbol{\sigma}^{int}$ are the stress tensors, $\boldsymbol{v}^{ext}$ and $\boldsymbol{v}^{int}$ the velocity fields and P^{int} and P^{ext} the pressure in the external and internal domains, respectively. The section S_i (resp. S_o) is located at a distance L from the cylindrical tube entrance (resp. exit). As shown in I, for large L the undisturbed pressure is uniform to $O(L^{-3})$, and the radial and axial velocities are $O(L^{-3})$ and $O(L^{-2})$ respectively. The pressure in S_i is kept constant and is set to zero. The section S_t is far enough inside the tube for entrance effects to be negligible and for Poiseuille flow to prevail. Furthermore, S_i, S_o and S_t

are also far enough from the capsule for the velocity perturbation to be negligible:

$$v^{ext} = v^{\infty} \approx 0 \quad \text{for} \quad x \in S_i \text{ or } S_o, \tag{2.3}$$

$$v^{ext}(x) = v^{\infty}(x) = 2(1 - r^2)e_x \quad \text{for} \quad x \in S_t, \tag{2.4}$$

$$P^{ext} = 0 \quad \text{for} \quad x \in S_i, \tag{2.5}$$

$$P^{ext} = P^{\infty} + \Delta P^+(t) \quad \text{for} \quad x \in S_o \quad \text{or} \quad S_t, \tag{2.6}$$

where e_x is the unit vector along the tube axis and ΔP^+ is the additional pressure drop due to the presence of the capsule. For Stokes flow, the entrance region in the tube has been found numerically to be of order one tube radius.

The no-slip boundary condition is required on the constriction wall:

$$v^{ext} = 0, \quad x \in B. \tag{2.7}$$

No-slip and membrane impermeability lead to

$$v^{ext} = v^{int} = \partial x/\partial t \quad \text{for} \quad x \in M. \tag{2.8}$$

Finally, dynamic equilibrium of the membrane is expressed as

$$\varepsilon(\sigma^{ext} - \sigma^{int}) \cdot n + p = 0 \quad \text{for} \quad x \in M, \tag{2.9}$$

where p is the force per unit area of deformed surface exerted by the membrane on the surrounding liquids. The capillary number ε:

$$\varepsilon = \mu V_0/E_s,$$

is a measure of the deformability of the membrane in terms of the ratio between viscous and elastic stresses. As ε decreases, the membrane becomes stiffer or the forces exerted by the fluids on the capsule decrease.

2.2. *Capsule membrane mechanics*

The principal directions of strain and stress are along the meridian and azimuth directions. Since the membrane is assumed to be infinitely thin, elastic stresses are replaced by tensions, with principal components T_s and T_ϕ in the meridian and azimuth directions. The shell equilibrium equations relate the elastic tensions to the tangential and normal components of the force per unit area p exerted by the membrane:

$$p \cdot \tau = \left[\frac{dT_S}{ds} + \frac{1}{r}\frac{dr}{ds}(T_S - T_\phi) \right], \tag{2.10a}$$

$$p \cdot n = -(K_S T_S + K_\phi T_\phi), \tag{2.10b}$$

where τ is the unit tangent vector to the meridian, oriented in the direction of increasing s and where K_s and K_ϕ are the principal curvatures of M:

$$K_S = -\left(\frac{d\tau_x}{ds}n_x + \frac{d\tau_r}{ds}n_r \right), \quad K_\phi = \frac{n_r}{r}. \tag{2.11a,b}$$

The membrane deformation is described in Lagrangian variables by labelling the membrane material points with their coordinates ξ, ρ, and arclength S before deformation ($S = 0$ at the first upstream point of the membrane where $\rho = 0$). After deformation, the points have coordinates x, r and arclength s ($s = 0$ where $S = 0$). The principal extension ratios λ_s and λ_ϕ in the meridian and azimuth directions are thus

$$\lambda_s = ds/dS; \quad \lambda_\phi = r/\rho. \tag{2.12a,b}$$

In order to close the problem, a constitutive law must be postulated for the membrane. In the particular case of an infinitely thin neo-Hookean three-dimensional incompressible material, the tensions are given by (Green & Adkins 1960, p. 153; Barthès-Biesel & Rallison 1981)

$$T_S = \frac{1}{3\lambda_s\,\lambda_\phi}\left(\lambda_s^2 - \frac{1}{\lambda_s^2\,\lambda_\phi^2}\right), \quad T_\phi = \frac{1}{3\lambda_s\,\lambda_\phi}\left(\lambda_\phi^2 - \frac{1}{\lambda_s^2\,\lambda_\phi^2}\right). \tag{2.13a,b}$$

Such a constitutive law allows for local surface area changes.

For a bilayer type of membrane, which strongly resists any change in the local surface area, the constitutive law of Skalak *et al.* (1973) is appropriate:

$$T_s = \frac{\lambda_s}{4\lambda_\phi}[\lambda_s^2 - 1 + C\lambda_\phi^2(\lambda_s^2\lambda_\phi^2 - 1)], \quad T_\phi = \frac{\lambda_\phi}{4\lambda_s}[\lambda_\phi^2 - 1 + C\lambda_s^2(\lambda_s^2\lambda_\phi^2 - 1)], \tag{2.14a,b}$$

where the ratio C between the dilatation and the Young modulus, is very large ($C \gg 1$). The relation between the surface Young modulus E_s and the surface shear modulus G_s depends on the constitutive law of the membrane. It is $G_s = E_s/3$ in the case (2.13) and $G_s = E_s/4$ in the case (2.14).

The problem is thus reduced to solving equations (2.2) with boundary conditions (2.3)–(2.9). The integration of the kinematic condition (2.8) gives the instantaneous position of the membrane points, and the force p is obtained from (2.10)–(2.12), subject to either (2.13) or (2.14).

3. Boundary integral formulation and numerical procedure

3.1. *Boundary integral formulation*

A convenient method for solving such creeping flow problems involving deformable interfaces is provided by the boundary integral formulation of the Stokes equations. This method was first proposed by Rallison & Acrivos (1978) for liquid drops in a pure straining motion, and later adapted to capsules in the same flow (Li *et al.* 1988, Pozrikidis 1990), to liquid drops in tubes (Martinez & Udell 1990) and to capsules in pores (I). This procedure will be only briefly outlined here, but details may be found in the book by Pozrikidis (1992) and in the related paper I. There are two main differences between the case in I and the present situation. First, the undisturbed velocity field is not known, and thus the use of disturbance fields is not beneficial. Secondly, some double-layer integrals must be added to account for the velocity fields at the entrance and exit fluid sections of the flow domain.

When the internal and external viscosities are equal, the integral equations greatly simplify and the cost of the computation is significantly reduced. This is the case that will be considered here, and from now on

$$\lambda = 1.$$

This assumption does not limit severely the conclusions of this study. Indeed it only affects the transient phases of the capsule motion as it enters or exits the pore. It does not influence the stationary results such as the steady capsule shape, velocity and pressure drop since, at steady state, the internal motion has ceased. Similarly, it would have also been possible to account for membrane viscoelasticity, by adding to either (2.13) or (2.14) a term of the form $\eta\partial\lambda_\alpha/\partial t$ where α stands for s or ϕ, and where η is the surface viscosity. For the same reason as above, the addition of this effect would not change the steady solution that is finally obtained. Like internal viscosity,

it would of course change the time (or equivalently the tube length) it takes to reach this steady state. Indeed, this was shown recently by Secomb (1995) who has studied the flow of tightly fitting capsules with a viscoelastic area-incompressible membrane through capillaries with variable cross-section.

The integral equation relates the velocity of points at M, B, S_f (S_f stands for S_i or S_o) and S_t to the velocities and forces on these surfaces:

$$\forall x \in M \cup \partial\Omega,$$

$$\frac{1}{\alpha}v(x) = -\int_{\partial\Omega} K(x-y)\cdot v(y)\cdot n(y)\mathrm{d}S(y) + \frac{1}{8\pi\varepsilon}\int_M J(x-y)\cdot p(y)\mathrm{d}S(y)$$

$$+ \frac{1}{8\pi}\int_{\partial\Omega} J(x-y)\cdot F(y)\mathrm{d}S(y), \tag{3.1}$$

where $\partial\Omega = B \cup S_f \cup S_t$. The parameter α is equal to 1 when x is on M or in Ω_{ext} and to 2 when x is on $\partial\Omega$. In the last integral, $F(y)$ denotes the traction exerted by $\partial\Omega$ on the suspending liquid. This is unknown on B and must be determined as part of the solution. On S_i, S_o and S_t, $F(y)$ follows from (2.3)–(2.6):

$$F(y) = 0 \quad \text{for} \quad y \in S_i,$$
$$F(y) = -(P^{np} + \Delta P^+)e_x \quad \text{for} \quad y \in S_o,$$
$$F(y) = -(P^{np} + \Delta P^+)e_x - 4re_r, \quad \text{for} \quad y \in S_t,$$

where the additional pressure drop is unknown.

The kernels J and K correspond respectively to the single- and double-layer potentials, and are known functions of position given in index notation by

$$J_{ij}(x-y) = \frac{\delta_{ij}}{|x-y|} + \frac{(x_i-y_i)(x_j-y_j)}{|x-y|^3}, \quad K_{ijk}(x-y) = \frac{-3}{4\pi}\frac{(x_i-y_i)(x_j-y_j)(x_k-y_k)}{|x-y|^5}$$

Correspondingly, the double layer integrals involving K, must be taken in the Principal Value sense.

Since the flow is axisymmetric, the ϕ dependence can be eliminated by analytical integration (Youngren & Acrivos 1975), reducing the dimension of the problem and converting the surface integrals into line integrals along meridian curves. The expression for the integrated kernels J can be found in Li *et al.* (1988) or in Pozrikidis (1992). Although the integrals in (3.1) are improper when $y = x$, due to the singular behaviour of the kernels J, they may be shown to exist because of the logarithmic behaviour of the singularity. The integrated kernels K are given by Youngren & Acrivos.

3.2. *Numerical procedure*

The numerical procedure for solving this problem follows closely that discussed in I, and is only briefly outlined. The entrance process is modelled as follows. The position of the capsule centre of mass at the channel axis is denoted $x_G(t)$. At time $t = 0$, the undeformed capsule is placed at $x_G(0)$, and its motion is followed through the pore. At any given time t, the position of the membrane material points is thus known, and the force p is obtained from (2.10)–(2.13) or (2.14). The boundary integral (3.1) is then written for points x on $\partial\Omega$, and use is made of boundary conditions (2.3), (2.4) and (2.7). The solution of the resulting Fredholm integral equation yields the force distribution exerted by the solid wall and the additional pressure drop on the outlet section S_t of the flow domain. Only the axial component of (3.1) is necessary to account for boundary condition (2.4). It follows that, when x is on S_t, the K kernel is identically

zero when y is also on S_t, and there is no singular contribution from the double-layer integrals. Once the forces on the boundary are known, the integral equation (3.1) is written for x on M, the velocity v^m of the membrane is computed. Equation (2.8) is integrated by means of the Euler method: the membrane points are moved by an amount $v^m \Delta t$ and the process is repeated. The program stops when the capsule reaches a steady state, i.e. when two values of the additional pressure drop corresponding to two positions one pore radius apart differ by less than 1%. The program also stops when the gap width between the capsule and pore wall becomes less than 0.01.

The exit process is modelled in essentially the same way. Starting with the steady shape obtained at the end of the entrance process, the capsule is placed at a position x_G far enough from the exit section for the presence of the exit funnel to be negligible and for Poiseuille flow to prevail in the pore downstream of the capsule. The solution of the integral equation then follows the same steps. The program stops when the additional pressure drop is reduced to less than 10% of its steady-state value.

A collocation technique is used, based on a partition of the boundaries and on the determination of the unknown forces and velocities at these discrete locations. The undeformed meridian curve of M is partitioned by n_M points evenly spaced by ΔS_M along the arclength. The meridian curve of B is partitioned with n_B points. These are evenly spaced by Δs_B in the cylindrical part. In the funnel part, they are evenly spaced along the parameter $x_B = \text{arccosh}(r_B)$ so that the last interval at the apex of the hyperbola is equal to Δs_B. During entrance, the flow pattern is essentially the same as in the hyperbolic pore studied in I. Consequently, the capsule and entrance section were positioned as in I, with typical values $L = 30$ and $x_G(0) = -6$. Section S_t is placed at a distance equal to at least 5 from the tip of the last steady capsule shape (this obviously implies some trial and error process) and is uniformly partitioned with a standard spacing $\Delta s_t = 0.03$. The singularities of the kernels $\boldsymbol{J}$ are treated as explained in I, by subtracting the asymptotic expression for $\boldsymbol{J}$ in the numerical integration of the singular terms and then adding the analytically calculated sum. The numerical integration is performed by means of Simpson's rule adapted to unequal intervals, which has an accuracy of order Δs^4, where Δs represents the maximum interval length. The corresponding weights depend only on the collocation point spacing.

The smoothing method of Longuet-Higgins & Cokelet (1976) is used to remove the oscillations in the capsule deformed profile. To ensure that the capsule volume remains constant, the position of the capsule points with respect to the centre of mass is rescaled by a factor equal to the cube root of the volume, at each time step. The relative volume variation between two successive time steps was always less than 10^{-6}. The geometrical properties of the capsule surface that enter equations (2.10)–(2.13) are evaluated by means of a five-point differentiation scheme with a precision $O(\Delta S_M^2)$ for the meridian curvature. The explicit character of the method (Euler time integration) makes it susceptible to numerical instabilities. Li *et al.* (1988) have introduced the following stability criterion:

$$\Delta t < \varepsilon \Delta S_M,$$

which leads to very small values for Δt.

3.3. *Numerical validation of the results*

When the cylindrical pore is sufficiently long, the capsule is expected to converge towards a steady shape with corresponding steady values of the additional pressure drop ΔP^{+ss} and of the centre-of-mass velocity v_{Gss}. The numerical solution is con-

n_M	85	101	147	171
ΔS_M	0.03	0.025	0.017	0.015
ΔP^{+ss}	7.49	7.12	6.95	6.89
$(v_x - v_G)_{max}$	0.34	0.22	0.12	0.09
$(v_r)_{max}$	0.32	0.21	0.12	0.09

TABLE 1. Effect of membrane partition on the additional pressure drop, relative axial and radial velocity. $R = 0.8$, $\varepsilon = 0.04$.

sidered to be acceptable when the values of ΔP^{+ss} obtained with two different partitions of the membrane and of the tube wall differing by at least 50% in point density, differ by less than 3% (it was found that v_{Gss} was not very sensitive to the precision of the results).

Typical results are given for an initially spherical capsule with radius 0.8, for capillary number $\varepsilon = 0.04$, and wall spacing $\Delta s_B = 0.08$, in table 1. The membrane is assumed to be of the neo-Hookean type and is described by (2.13). On figure 2, the evolution of ΔP^+ with the position of x_G along the channel is shown for $n_M = 85$, 101, 147 and 171, corresponding to $\Delta S_M = 0.03$, 0.025, 0.017 and 0.015. The exact steady-state value of the additional pressure drop is very close to 6.9. The coarser partition does not satisfy the accuracy criterion, whereas the three finer partitions do. The corresponding steady profiles are shown on figure 3. Except for the coarser partition, they are superimposed within graphical precision. However, it is interesting to note that for the evaluation of ΔP^+ during the entrance phase, a coarse partition is quite sufficient (figure 2). Indeed, the principal cause for error is due to the computation of the membrane curvature which takes its maximum value in the tube.

A further check on precision consists in evaluating the radial velocity of the membrane as well as the difference between the values of the axial velocity of the membrane and the centre-of-mass velocity v_G (figure 4*a, b*). At steady state both quantities should be zero for all collocation points on the membrane. Those two components of velocity are very small everywhere on the membrane except where the curvature is large and changes sharply. However, the shape of the capsule remains steady (i.e. the coordinates of the membrane collocation points remain constant within 10^{-8} for 10 000 time iterations). This is due to the fact that the disturbing effect of the non-zero velocity field is balanced by both the volume correction and the smoothing procedure. Even though the largest value of the velocity deviation may seem unacceptably large, the model gives acceptable results based on pressure drop and shape convergence. This indicates that small errors in the profile geometry (specifically, in the curvature) lead to comparatively large errors in the local membrane velocity, but do not influence significantly the overall perturbation to flow as measured by the additional pressure drop. A similar observation was made by Halpern & Secomb (1989) for tightly fitting capsules. It can be easily checked that the maximum error on the velocity behaves as ΔS_M^2. In order to reduce the error by a factor of 4, the collocation point density must be doubled and the time step correspondingly halved. This leads to unacceptably large computation times. Consequently, the evaluation of the accuracy of the results in this paper will be systematically based on the steady pressure drop. The effect of a finer partition of the solid boundary was also investigated, by decreasing Δs_B by 75%. The concomitant change in ΔP^{+ss} was less than 1%.

The validity of condition (2.4) has also been checked. The axial flow velocity upstream of the capsule was computed by means of the integral equation (3.1)
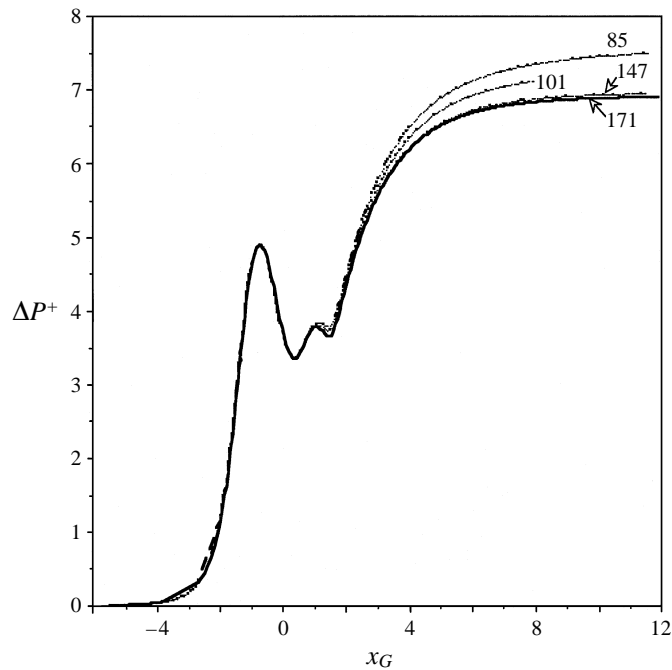
FIGURE 2. Additional pressure drop as a function of x_G for four partitions of the membrane with respectively 85, 101, 147 and 171 collocation points. $R = 0.8$, $\varepsilon = 0.04$.
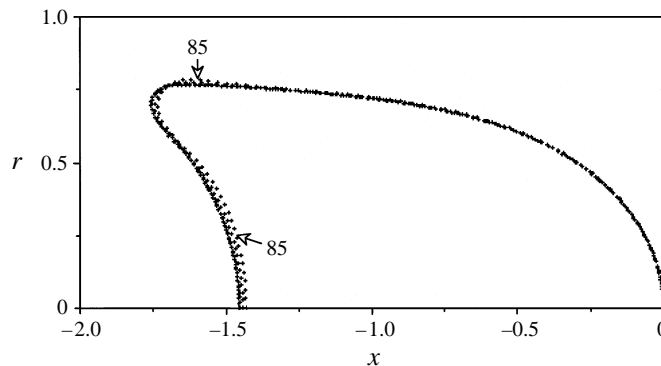

FIGURE 3. Half-capsule profiles for four partitions of the membrane with respectively 85, 101, 147 and 171 collocation points. $R = 0.8$, $\varepsilon = 0.04$.

evaluated for x in Ω_{ext} and located on the tube axis. It is found that the Poiseuille velocity is recovered within 1% at a distance roughly equal to one tube radius from the capsule tip. Since section S_t is always at least at a distance equal to 5 tube radii from the capsule, it may be safely assumed that (2.4) is fulfilled. Furthermore, this shows that the pressure drop due to a train of capsules is simply the sum of the individual pressure drops due to each capsule as if it were travelling alone in the tube, provided the distance between two successive particles is at least one tube diameter.

   The practical limitations of the numerical model are of two types. For tightly fitting capsules, the deformation of the membrane is large, and thus ΔS_M must be small enough for the metric properties of the membrane to be determined with satisfactory
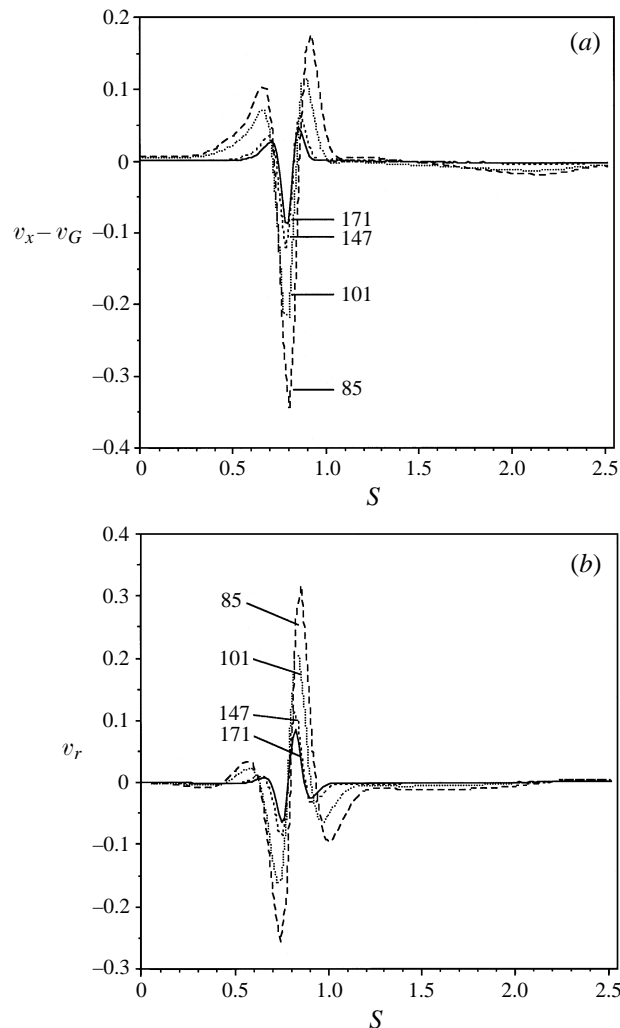
FIGURE 4. Membrane velocity for four partitions of the membrane with respectively 85, 101, 147 and 171 collocation points. $R = 0.8$, $\varepsilon = 0.04$. (*a*) Relative axial velocity, (*b*) radial velocity.

precision. Furthermore, large hydrodynamic forces appear in the film region, and a small partition of the tube wall must be used. The *ad hoc* criterion used here was that the spacing of collocation points on the wall should be less than half the film thickness. For very small gaps, it is probably more efficient to use the lubrication approximation, at least in the film region, but our model is not at present designed to do so. The other limitation is linked to the appearance of a locally large curvature, which is difficult to compute with precision. In such zones, the membrane hypothesis must fail and some bending resistance should be introduced at least locally. This has not yet been incorporated into the present model.

4. Motion of a spherical neo-Hookean capsule

Results are presented for initially spherical capsules (initial radius R) with a neo-Hookean constitutive law given by (2.13*a,b*). The cases of a 'small' ($R = 0.8$) and
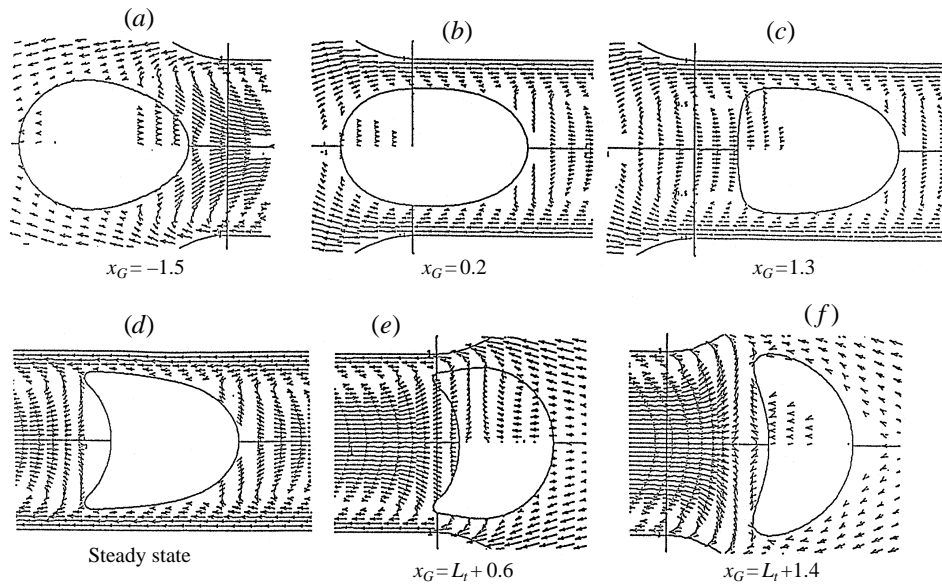
FIGURE 5. Successive capsule profiles and flow field in the capsule reference frame. Only velocities larger than 0.1 are shown. $R = 0.8$, $\varepsilon = 0.04$.

of a 'large' ($R = 1.2$) capsule are considered separately. The possible occurrence of break-up is discussed. Additional results are given by Quéguiner (1995).

4.1. *Small capsule: $R = 0.8$.*

As an example the flow of a capsule with $R = 0.8$ is discussed in detail for a value of $\varepsilon = 0.04$ such that a significant deformation is reached at steady state. The successive capsule profiles and the velocity distribution in a reference frame moving with the capsule centre of mass, are shown on figure 5. The velocity distribution shows the coupling between the internal and external flows. The capsule first takes an oblong shape upstream of the tube entrance ($x_G < 0$), while the internal liquid has a forward motion near the tip (figure 5a). However, this shape is not in equilibrium with Poiseuille flow, and the steady profile that is finally obtained is 'parachute' like (figure 5d). Once the capsule has entered the tube ($x_G > 0$), the external and internal velocities are directed inwards at the rear of the capsule. This eventually leads to the concave shape of this region (figure 5b, c). At steady state, the internal velocity vanishes, and the capsule behaves as an undeformable particle. Poiseuille flow is recovered within about one tube radius from the particle (figure 5d). The corresponding distributions of meridional tension are shown on figure 6. When the capsule is still in the funnel ($x_G = -1.5$), the front part is significantly extended, but the rear only a little. When the centre of mass is just inside the tube ($x_G = 0.23$), the extension of the front has increased, whereas the rear is essentially slack. At steady state, the maximum extension is located near the front and the rear is slightly extended because of the local concavity. A small zone of compression appears near the edge of the capsule where the curvature is locally large. It is in this zone, that bending forces are expected to become important.

The additional pressure drop as a function of the position of the capsule centre of mass x_G along the axis is shown on figure 7. The pressure drop increases sharply as the capsule approaches the entrance of the tube. A local peak occurs before the capsule
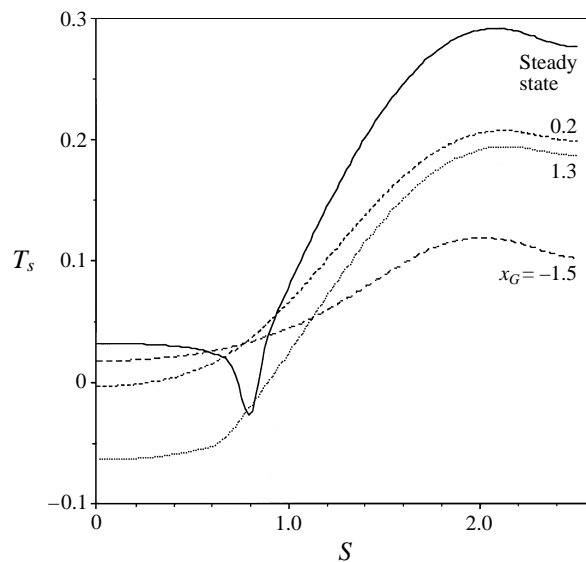
FIGURE 6. Meridional tension distribution during entrance process, for $x_G = -1.5$, 0.2, 1.3 and for steady state. $R = 0.8$, $\varepsilon = 0.04$.

has entered the constriction. This is caused by the partial plugging of the channel during the initial deformation process. A similar phenomenon has been reported by Secomb (1995) and by Secomb & Hsu (1995) for the flow of cells in a varying-cross-section capillary. The following decrease in pressure drop is due to the cooperative effect of the membrane tensions that have built up during the entrance phase. On the same graph is shown the corresponding pressure drop curve that is obtained in the hyperboloidal constriction of I. Since the two curves coincide during the entrance phase, the discussion of the main physical phenomena provided in I also applies here. In particular, the variations of the pressure drop near the entrance ($x_G \approx 0$), may be attributed to successive phases of elastic tension relaxation and build up. Another conclusion that may be drawn from this comparison is that the hyperboloidal constriction is useful for the study of entrance phenomena even in long pores.

Starting with the steady state obtained above, the exit process from the tube can be modelled. The corresponding capsule profiles and velocity fields are also shown on figure 5. The capsule is 'blown out' from the tube: as the front part slows down, the rear part still advances with the tube flow velocity. There are two converging internal flows coming from the front and from the rear of the capsule (figure 5e). The capsule thus expands in the radial direction and the parachute shape becomes even more pronounced (figure 5f), before the capsule eventually resumes its spherical shape. A similar exit process has also been observed in the hyperboloidal constriction. The corresponding pressure evolution curve is shown on figure 7. The local exit peak is due to the blowing out process and to the fact that for a short time, the capsule tends to block partially the exit flow from the tube. Altogether, the motion of the capsule through the tube is a viscoelastic process, since it results from the interplay of viscous and elastic forces. As a consequence, the entrance and exit pressure curves are not symmetric even though the flow is inertialess.

The steady-state shapes in the cylindrical section, obtained for $R = 0.8$ and for different values of ε are shown on figure 8. The capsule deformability increases with
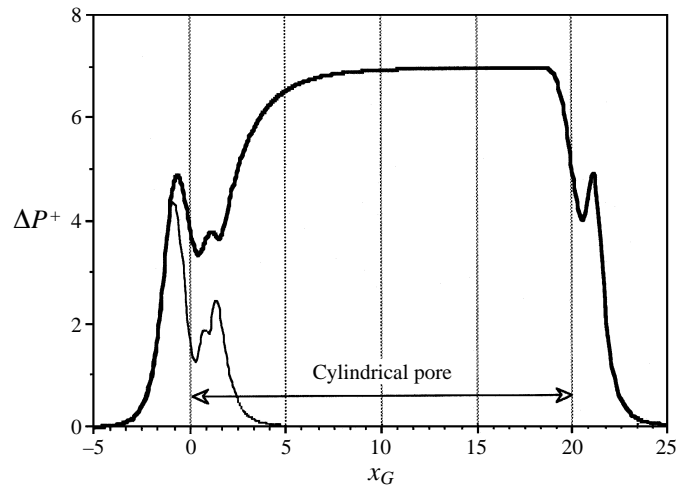
FIGURE 7. Additional pressure drop evolution during flow. Comparison between a long cylindrical pore (━━) and a short hyperbolic pore (——). $R = 0.8$, $\varepsilon = 0.04$.

ε. For infinite values of ε, it is clear that no steady state can exist. The 'membrane' is then just a collection of fluid particles that are convected with the flow, and the deformation grows indefinitely. Correspondingly, for large values of ε, a steady state of the capsule could not be obtained. The nature of the problem can be ascertained from the behaviour of the meridional extension ratio λ_s. This ratio reaches a maximum λ_{smax} at the front tip of the capsule. The variations of λ_{smax} are plotted on figure 9 as a function of x_G. For small values of ε, a steady value of λ_{smax} is reached; this is not the case for $\varepsilon = 0.05$, even after severely refining the membrane partition. It seems that we are faced with the phenomenon of continuous deformation which is predicted for liquid drops (see the review paper by Stone 1994) and for capsules (Li *et al.* (1988)) and which leads to bursting of the particle. This is an interesting prediction of the model, since bursting occurs because the membrane forces cannot balance the viscous forces. During the continuous extension, the curvature of the parachute edge also grows without bound. A non-zero bending resistance would oppose this but would not prevent the continuous extension of the upstream tip. The model predictions are consistent with experiments on liquid drops in tubes (Olbricht & Kung 1992) where break-up is observed due to the penetration of a liquid jet into the rear part of the drop. This is analogous to what is predicted here.

When ε is reduced, the capsule becomes less deformable and this leads to an increase in the steady-state pressure drop ΔP^{+ss} (figure 14). The asymptotic limit $\varepsilon = 0$, corresponding to a solid sphere, was computed by Hyman & Skalak (1972). For $R = 0.8$, the asymptotic values of ΔP^{+ss} and of the relative particle velocity $(v_{Gss} - 1)$ are respectively 7.74 and 0.27. For the smallest value of ε investigated here ($\varepsilon = 0.005$), the numerical value of $(v_{Gss} - 1)$ is 0.28, which is close to the asymptotic value. However, the numerical value of ΔP^{+ss} is 8.1, which is also close but larger than the asymptote. It would thus seem that the asymptotic value of the pressure drop is approached from above. This result was consistently observed for all capsules with $R \leqslant 0.8$, where the steady pressure drop first increases with ε and then decreases.

This phenomenon is due to the flared profile that the particle must take to balance fluid forces (figure 8). For small ε, the gap width between the wall and the capsule or the sphere is of the same order. However, the gap length is longer for the capsule

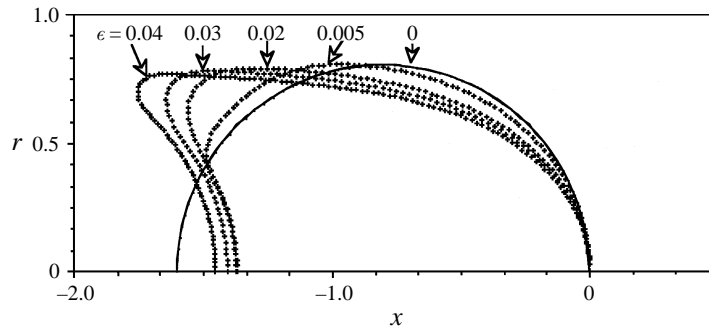FIGURE 8. Effect of capillary number ε on the steady shape of a spherical capsule with $R = 0.8$. The numbers indicate the corresponding values of ε.
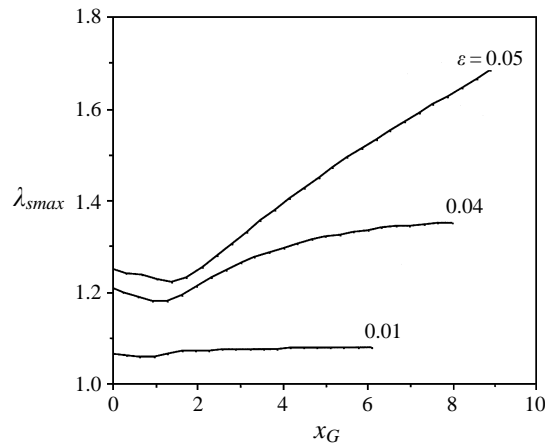

FIGURE 9. Evolution of the maximum meridional elongation ratio as a function of position along the pore. For $\varepsilon \leqslant 0.04$, a steady state is reached. For $\varepsilon = 0.05$ the elongation ratio of the membrane increases without limit, thus indicating the occurrence of burst through continuous elongation. $R = 0.8$.

than for the sphere (because of the concave region at the back of the capsule). It follows that the perturbation created by the capsule is larger than the one created by the sphere. For larger values of ε, the gap width between the capsule and the wall becomes larger than for the sphere. Even though the gap length is longer, the overall dissipation created by the capsule is less than that for the sphere.

4.2. *Large capsule: R = 1.2*

The case of a capsule with $R = 1.2$, $\varepsilon = 0.005$ is taken as an example. The different phases of entrance and exit are quite similar to those observed for small capsules (figure 10). During entrance, the internal liquid has a diverging motion towards the front and towards the rear, which leads to the deformation of the sphere into a slug. During exit, the internal fluid converges from the front and from the back of the capsule, thus leading to a radial expansion of the slug. The pressure drop evolution as a function of x_G during entrance and exit is shown on figure 11. Again, two local peaks of pressure occur in the entrance and exit funnels. They are both due to transient partial plugging of the tube. The entrance peak can be as high as the
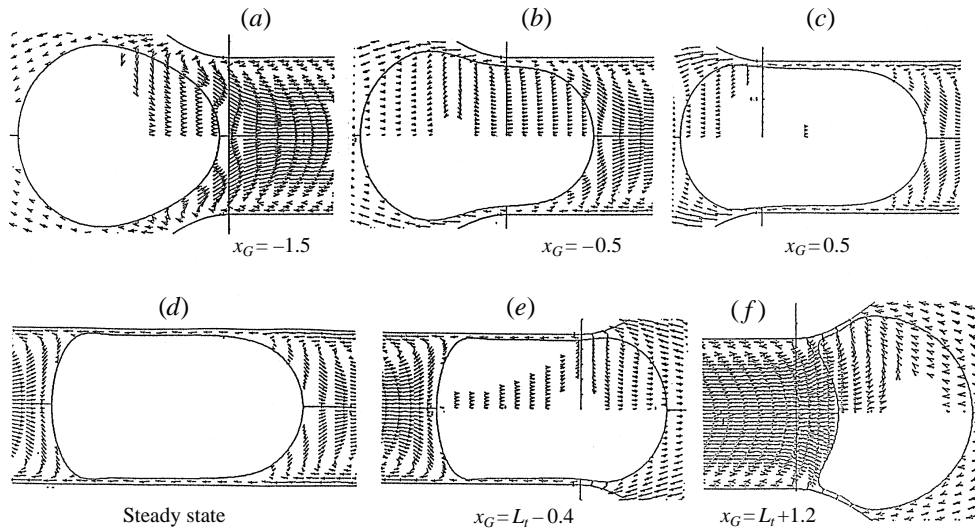
FIGURE 10. Successive capsule profiles and flow field in the capsule reference frame. Only velocities larger than 0.1 are shown. $R = 1.2$, $\varepsilon = 0.005$.
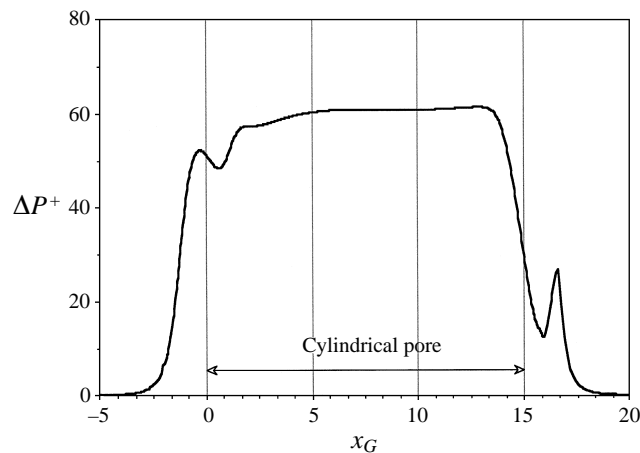

FIGURE 11. Additional pressure drop evolution during flow. $R = 1.2$, $\varepsilon = 0.005$.

steady plateau value. The steady additional pressure drop is much larger than that for $R = 0.8$.

The steady capsule profiles obtained for different values of ε are shown on figure 12. The rear of the capsule is convex for small ε, and becomes concave as ε increases. For ε equal to 0.015, no steady state can be obtained and the phenomenon of continuous extension is also observed. As ε decreases, the steady pressure drop increases sharply, the film thickness decreases and the centre-of-mass velocity also decreases towards the asymptotic value of unity.

It is of interest to compare the model predictions with the results obtained by Halpern & Secomb (1989) for area-incompressible capsules based on the lubrication approximation. In the case where the shear resistance of the membrane is neglected, the membrane behaviour becomes essentially Eulerian, the elastic tensions are isotropic and the meridional extension ratio can be obtained in a simple way.
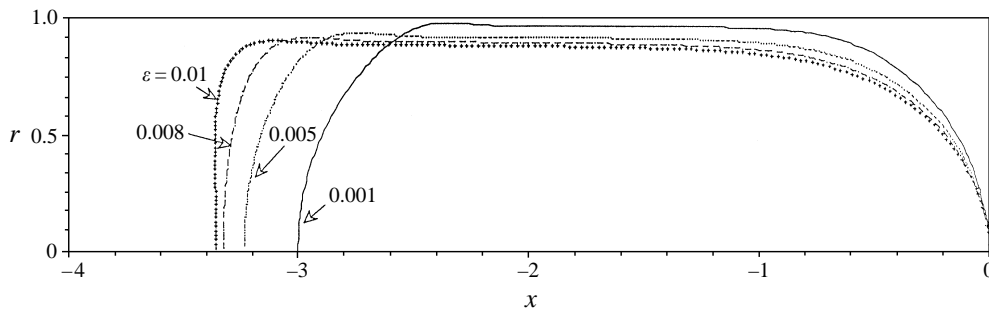
FIGURE 12. Effect of capillary number ε on the steady shape of a spherical capsule with $R = 1.2$. The numbers indicate the corresponding values of ε. For small values of ε, the back of the capsule is convex.
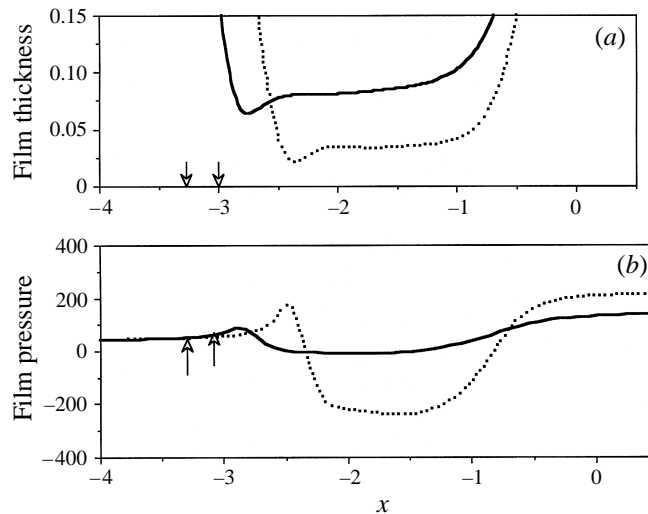

FIGURE 13. Detail of the film thickness (*a*) and of film pressure distribution (*b*) for two values of ε: 0.005 (——) and $\varepsilon = 0.001$ ($\cdots$). In both case the tip of the capsule is positioned at $x = 0$. Arrows indicate the position of the back of each capsule.

The centre of the capsule is surrounded by a constant-thickness film. The pressure in the film and the tension in the membrane are then linear functions of the arclength, i.e. of x in the film region. Details of the film profile for $R = 1.2$ and neo-Hookean capsules are shown on figure 13(*a*). The classical oscillation of the film near the rear of the capsule is recovered by the model. However, the film thickness is not constant but increases as one moves from the back to the front. Thus the capsule behaves as a slipper bearing: the pressure in the film goes through an extremum (figure 13*b*). The pressure evolution as well as the capsule profile are different from those obtained by Secomb *et al.* (1986) for area-incompressible cells with shear and bending resistance. This shows that the membrane constitutive equation plays an important role in the control of capsule dynamics. A full lubrication analysis would be difficult to perform for a neo-Hookean capsule, since the mapping between the undeformed and deformed profiles is not simple and must be obtained numerically by means of some kind of iterative method. Consequently, the present model where entrance into the tube is specifically taken into account, is *essential in*
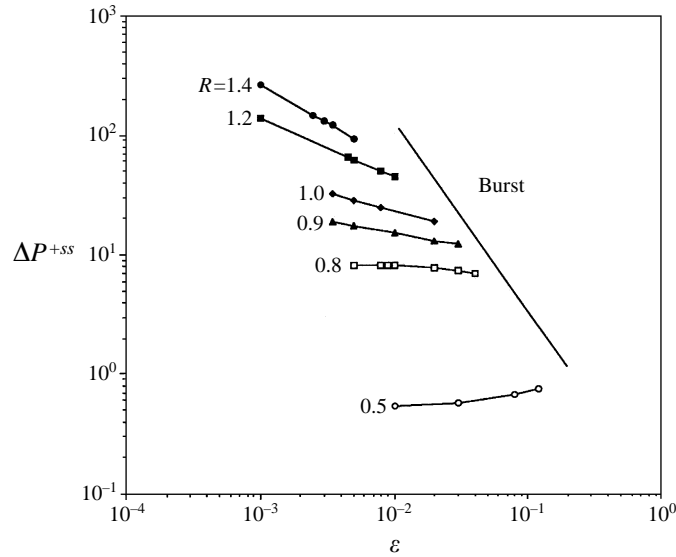
FIGURE 14. Steady pressure drop due to a spherical neo-Hookean capsule, for $R = 1.4$; 1.2; 1.0; 0.9; 0.8; and 0.5. Burst occurs when ε exceeds a critical value that depends on size.

the sense that it provides the necessary mapping between the reference and deformed states.

5. Spherical neo-Hookean capsule: global effect of size and rigidity

The steady results obtained for neo-Hookean initially spherical capsules with radii ranging from 0.5 to 1.4 are now summarized. Smaller capsules are not very interesting to study, as they create a very small hydrodynamic perturbation. Capsules larger than $R = 1.4$ tend to fill the tube and leave a gap that is too narrow for the present computation to be accurate (see discussion in §3.3). The steady additional pressure drop ΔP^{+ss} is shown as a function of R and ε in figure 14. The pressure drop in the absence of the capsule is simply

$$\Delta P^{\infty} = 8(L_t + L'),$$

where L' accounts for entrance and exit effects. A typical filtration membrane has L_t of order 5 or more. Consequently, a small capsule such that $R \leqslant 0.8$ creates a relative perturbation that is less than 20%, and as such, difficult to measure with precision. Furthermore, for small capsules ($R < 1$), it appears that ΔP^{+ss} is sensitive to size effects but insensitive to the membrane elasticity as measured by ε. For example, for $R = 0.9$, a two-fold increase in ε leads to a concomitant decrease in ΔP^{+ss} of about 15%. The same conclusion is reached by Drochon *et al.* (1993) who conducted filtration experiments (pore diameter 5 µm) on red blood cells suspended in Dextran solutions such that the viscosity ratio λ is of order unity. They find that the filtration time of normal and membrane rigidified cells (with E_s roughly doubled) differed by 10 to 20%.

For large capsules ($R \geqslant 1$), the relative pressure drop is large enough to be measurable. Furthermore, the effect of membrane rigidity is important. Indeed, for $R = 1.2$, a two-fold increase in ε leads to a decrease in ΔP^{+ss} of about 62%. This indicates that filtration experiments may be used to measure the elastic modulus of
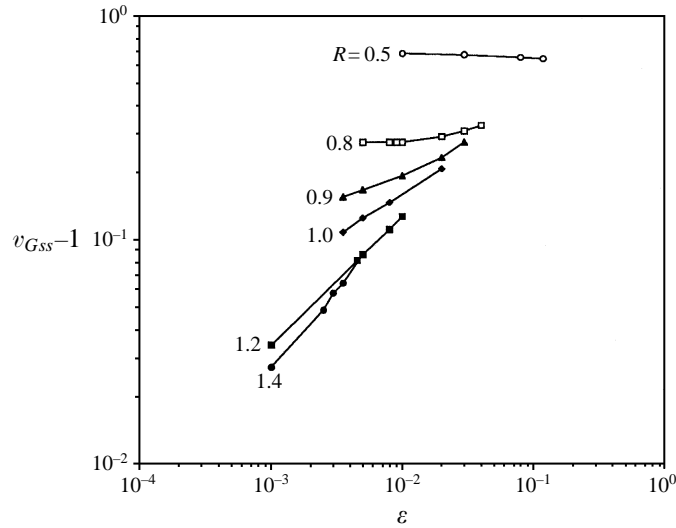
FIGURE 15. Steady relative velocity of a spherical neo-Hookean capsule. Same R values as figure 14.

the membrane, provided that relatively small pores are used, so that a significant deformation of the capsule occurs. Break-up through the phenomenon of continuous extension is consistently observed for all capsules, and the limit between steady and unsteady cases is indicated on figure 14. As expected, the larger the particle, the smaller the critical value of ε.

The relative capsule velocity is shown on figure 15. All capsules flow faster than the mean velocity of the suspending liquid, since $(v_{Gss} - 1)$ is positive. For large capsules, this quantity becomes very small, as slugs tend to move with the mean flow velocity. If the tube is fed with a capsule suspension, dilute enough to avoid interaction effects, the particle concentration ϕ_t inside the tube will thus be smaller than the feed ϕ_f concentration in the reservoir (Sutera *et al.* 1970):

$$\phi_t / \phi_f = 1 / v_{Gss}.$$

This is the Farheus effect, first observed for capillary blood flow. Obviously, this effect is more prominent for small than for large capsules.

For large capsules such that $R \in [1.0, 1.4]$, the particle takes a slug shape, and both ΔP^{+ss} and $(v_{Gss} - 1)$ follow power laws with respect to ε, with a good approximation. Indeed, in the range of parameters that has been tested, it is found that:

$$\Delta P^{+ss} = k\varepsilon^{-n}, \tag{5.1}$$

$$(v_{Gss} - 1) = k'\varepsilon^{n'}, \tag{5.2}$$

where k, k', n and n' depend on R and are given in table 2 together with the correlation coefficient. Such approximate formulae are useful for the interpretation of filtration experiments through long enough pores, where the pressure drop and the flow rate across the filter are simultaneously measured.

Another quantity of interest is the length of tube L_e necessary to reach a steady state. The entrance length is defined as the position of the capsule front where the steady value of ΔP^{+ss} has been reached within 3%. For very deformable particles, the larger the capsule, the longer the entrance length. As shown on figure 16, for small values of ε, the interplay between size and rigidity is complex. Owing to geometrical

R	k	n	Regr.	k'	n'	Regr.
0.8	5.48	0.08	0.898			
0.9	5.91	0.20	0.998	0.64	0.26	0.984
1.0	5.87	0.30	1.000	0.86	0.37	0.999
1.2	4.34	0.50	1.000	1.72	0.57	1.000
1.4	3.19	0.64	0.999	3.53	0.71	0.997

TABLE 2. Power-law coefficients for the additional pressure drop (k, n) and for the relative capsule velocity (k', n'), with the associated regression coefficients
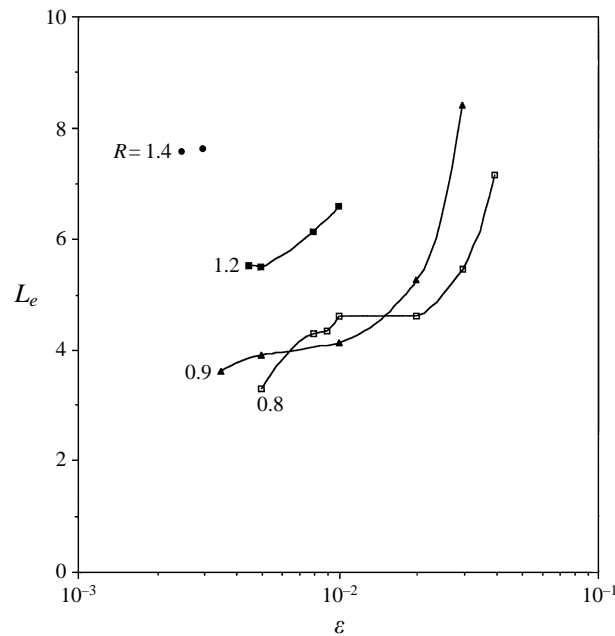

FIGURE 16. Entrance length of a spherical neo-Hookean capsule. Same R values as figure 14.

constraints, large capsules take the equilibrium slug shape at the beginning of the pore, but need a minimum length to just squeeze in. The entrance length of small capsules is of order 3.5 to 5 pore radii, and increases sharply as ε approaches the critical break-up value. For large capsules the entrance length is quite large (from 5.5 to 8). These results indicate that, unless the pore is long enough, filtration of cells or capsules is an essentially transient process that cannot be analysed in a simple fashion. Indeed, a typical membrane used for red blood cell filtration has pores with a diameter of 5 μm and a length between 10 and 15 μm (Fisher *et al.* 1992, Drochon *et al.* 1993). In such a membrane, a steady flow situation is probably not reached.

6. Influence of membrane constitutive behaviour

We now consider discoidal capsules (denoted C_{SK}) with a membrane that resists local area changes and is thus described by equations (2.14*a*, *b*). Interface mechanics depend on two parameters: the elastic modulus E_s (measured by ε) and the
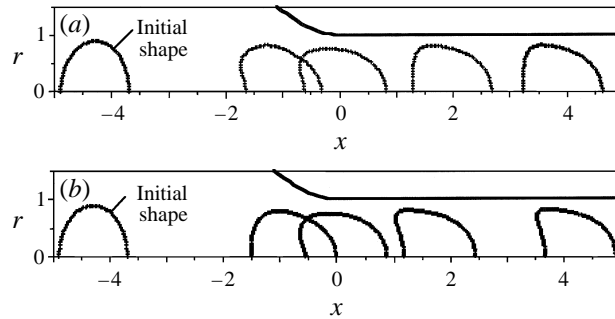
FIGURE 17. Successive half-profiles of a spheroidal capsule during entrance. $R = 0.9$, $D = 0.6$, $\varepsilon = 0.02$. (*a*) C_{SK}, (*b*) C_{NH}.
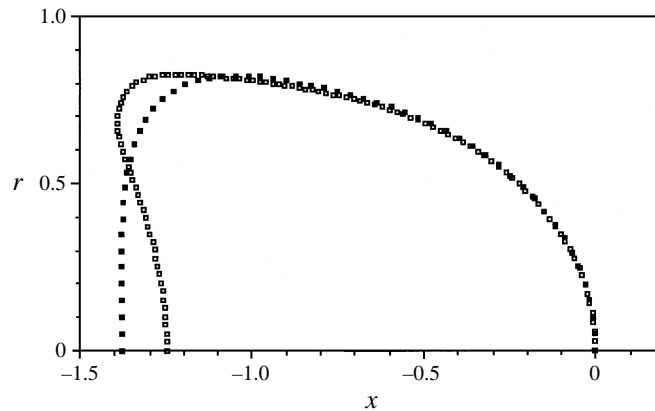

FIGURE 18. Steady-state shapes. $R = 0.9$, $D = 0.6$, $\varepsilon = 0.02$. C_{SK} (■); C_{NH} (□).

relative area dilatation modulus C. Two cases are studied: a small capsule with $R = 0.9$, $D = 0.6$ and a large capsule with $R = 1.2$, $D = 0.8$. Thinner capsules with a smaller sphericity index (ratio between the surface of the sphere that has the same volume and the surface of the particle) tend to buckle, and could not be modelled.

6.1. *Small capsule (* $R = 0.9$, $D = 0.6$ *)*

The effect of the membrane constitutive law is assessed by comparing the flow of two capsules C_{NH} and C_{SK} which have the same initial geometry ($R = 0.9$, $D = 0.6$), but with membranes obeying respectively equations (2.13*a*,*b*) and (2.14*a*,*b*). The parameter C is set to 60 for C_{SK}, and in both cases the capillary number is $\varepsilon = 0.02$. The successive profiles of the particle as it flows into the pore are shown on figure 17(*a*,*b*). It appears that the constraint imposed on surface area limits the deformation of C_{SK}. As a consequence, the back of C_{SK} is not concave like that of C_{NH} (figure 18). The steady additional pressure drop is respectively 9.3 for C_{NH} and 8.8 for C_{SK}. These two values are very close. This shows again that the details of the deformed geometry do not influence much the hydrodynamic perturbation created by the capsule. The value of ΔP^{+ss} is slightly larger for C_{NH} than for C_{SK}. This is due to the fact that the film region of C_{NH} is longer than that of C_{SK}, owing to the negative curvature region at the rear of the capsule.
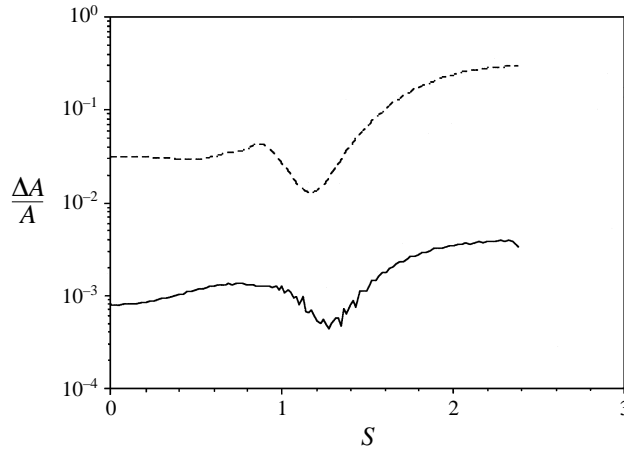
FIGURE 19. Steady distribution of local area change along the meridian. $R = 0.9$, $D = 0.6$, $\varepsilon = 0.02$. ——, C_{SK}, - - -, C_{NH}.
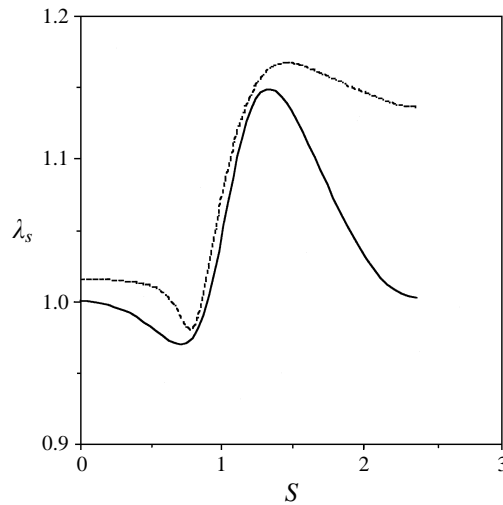

FIGURE 20. Steady distribution of meridional tension. ——, C_{SK}; - - -, C_{NH}. $R = 0.9$, $D = 0.6$, $\varepsilon = 0.02$. For C_{SK}, λ_s must be equal to 1 at both extremities.

The relative local area dilatation is simply given by

$$\Delta A / A = \lambda_s \lambda_\phi - 1.$$

The steady-state value of $\Delta A/A$ is shown on figure 19. For C_{SK} it is everywhere very small, with a maximum value of order 0.4%. In the case of C_{NH}, the local area dilatation is large with a maximum of about 30% occurring near the tip of the capsule. It is also of interest to compare the steady-state distribution of the meridian extension ratio λ_s (figure 20). C_{SK} is slightly compressed at the rear and extended near the front. At the two tips, where $\lambda_s = \lambda_\phi$, there should not be any extension. Even though the C_{SK} deformation is locally significant ($\lambda_s \approx 1.1$), its area is nevertheless nearly constant. C_{NH} is extended everywhere, except locally near the edge of the parachute. The rear is also extended because of the concavity.
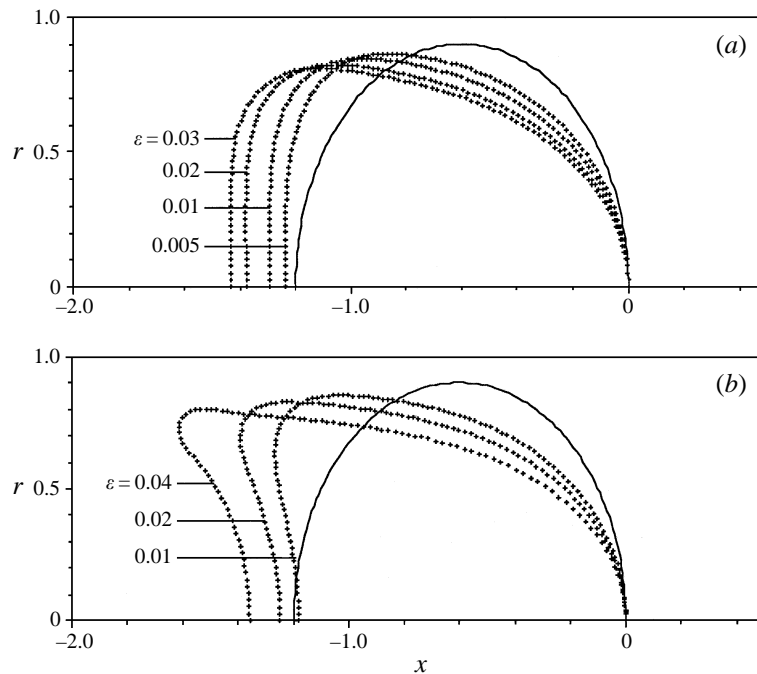
FIGURE 21. Effect of capillary number ε on the steady shape of a spheroidal capsule with $R = 0.9$, $D = 0.6$. The numbers indicate the corresponding values of ε. (*a*) C_{SK}, (*b*) C_{NH}.

The effect of area dilatation can also be assessed by comparing results obtained for C_{SK} with different values of C ($C = 10, 60, 90$) and $\varepsilon = 0.02$. The corresponding values of the maximum area dilatation are then $\Delta A/A = 2.1, 0.4$ and 0.25%. However, the steady additional pressure drop remains almost constant ($\Delta P^{+ss} = 10.1, 10.2, 10.2$). This means that a fully area-incompressible capsule would create essentially the same amount of additional pressure drop and would have the same profiles as those for C_{SK} shown in figure 17.

The effect of capillary number on the capsule shape is shown on figure 21(*a, b*). The steady profiles of C_{SK} are obtained for different values of ε, but for the same value of maximum area dilatation set to 0.4% (they thus pertain to a nearly area-incompressible capsule). The rear of the capsule is not concave, even for very deformable particles, corresponding to fairly large values of ε. Furthermore, the capsule shape does not change much as ε is increased. This indicates that for large values of ε, a steady state is reached where the mechanics of the capsule are essentially dominated by area compressibility. The neo-Hookean capsule C_{NH} exhibits a different behaviour: the rear always shows some concavity. Furthermore, as ε is increased past 0.04, C_{NH} undergoes continuous elongation and bursts. This phenomenon does not occur with C_{SK}, since the resistance to area dilatation limits the overall deformation of the capsule. This does not mean that break-up would not occur for C_{SK}, but the burst criterion in that case would have to be based on some critical stress level in the membrane.

The steady pressure drop evolution for C_{SK} and C_{NH} is shown on figure 22. The two curves follow the same trend and are almost superimposed for small values of ε, such that the shear resistance of the membrane is prevalent. For ε larger than about 0.04, C_{NH} seems to burst, whereas C_{SK} reaches an asymptotic state controlled
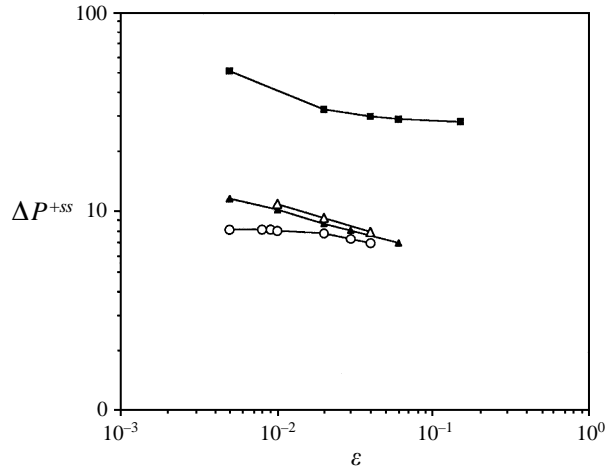
FIGURE 22. Global effect of geometry and membrane behaviour on steady pressure drop. Discoidal capsule $R = 0.9$, $D = 0.6$: ▲, C_{SK} with maximum area change of 0.4%, △, C_{NH}; ○, equal-volume spherical capsule with neo-Hookean membrane $R = 0.8$. Discoidal capsule $R = 1.2$, $D = 0.8$: ■, C_{SK} with maximum area change of 1.5%

by area incompressibility. It is also of interest to compare the pressure drops due to two roughly isovolumic neo-Hookean capsules which are initially spherical ($R = 0.8$) or discoidal ($R = 0.9$, $D = 0.6$). The discoidal capsule creates a larger pressure drop than the spherical one (figure 22). This may be due to the 'excess' surface area of the discoidal particle. However, as ε increases, the difference between the two pressure drops decreases. This means that the influence of the initial geometry fades out until burst occurs.

6.2. *Large capsule ($R = 1.2$, $D = 0.8$)*

A large area-incompressible capsule must have a large enough sphericity index to flow into the tube. In a very small cylindrical tube, the limiting shape the capsule can take is that of a cylinder closed by two hemispherical caps. It is then straightforward to determine the critical minimum radius of the tube into which the capsule can squeeze while keeping constant its *global* volume and surface. In the case of the spheroidal capsule $R = 1.2$, $D = 0.8$, the corresponding critical tube radius is 0.875. Consequently, it may be hoped that this capsule can deform enough to fit in a tube with unit radius. For a given value of ε, as $C \to \infty$ the membrane becomes fully area incompressible. The maximum area dilatation $(\Delta A/A)_{max}$ should tend to zero asymptotically, and the additional pressure drop ΔP^{+ss} should reach an asymptotic value, as was found by Halpern & Secomb (1989) for closely fitting area-incompressible capsules.

The flow of a capsule C_{SK} ($R = 1.2$, $D = 0.8$) has thus been studied in detail for $\varepsilon = 0.04$ and different values of C (table 3). The variations of ΔP^{+ss} and of $(\Delta A/A)_{max}$ are plotted as functions of a modified capillary number associated with area dilatation, $\varepsilon' = \varepsilon/C$ (figure 23). As ε' goes to zero, ΔP^{+ss} increases without showing any tendency to level off at an asymptotic value. However $(\Delta A/A)_{max}$ decreases with ε' (for the smallest value $\varepsilon' = 4.4 \times 10^{-5}$, the maximum local area change is 0.4%, at the limit of numerical accuracy). It may be expected that $(\Delta A/A)_{max}$ goes to zero as $\varepsilon \to 0$. Indeed, as was pointed out by Professor R. Skalak (private communication), it is always possible to map continuously an axisymmetric surface onto another axisymmetric surface keeping the local surface area constant (see the Appendix for

ε	C	ε' ($\times 10^4$)	$(\Delta A/A)_{max}$	ΔP^{+ss}
0.02	90	2.2	1.4%	32.1
0.04	120	3.3	2.0%	27.7
	160	2.5	1.6%	28.0
	240	1.7	1.2%	29.6
	500	0.8	0.7%	32.0
	900	0.4	0.4%	35.1
0.06	160	3.7	2.2%	26.1
	300	2.0	1.4%	28.6
0.15	800	1.9	1.4%	27.7
	1600	0.9	0.8%	29.6

TABLE 3. Effect of ε and C on the flow of a large ellipsoidal capsule ($R = 1.2$, $D = 0.8$)
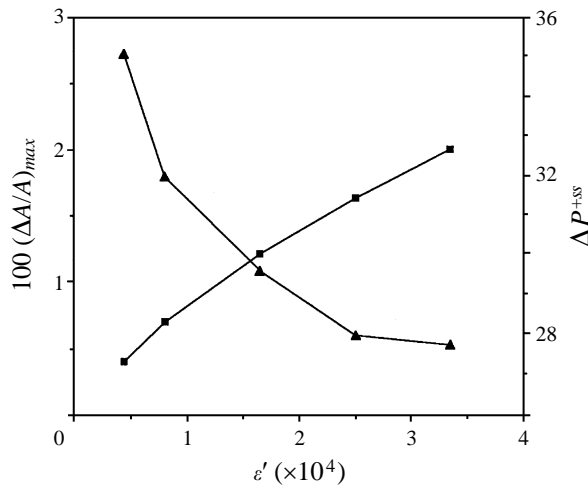

FIGURE 23. Spheroidal capsule ($R = 1.2$, $D = 0.8$): effect of ε' on the steady additional pressure drop (▲) and on the maximum area dilatation with $\varepsilon = 0.04$ (■).

proof). However, the fact that ΔP^{+ss} does not seem to reach any asymptotic value indicates that the capsule $R = 1.2$, $D = 0.8$, cannot flow into the tube, while keeping its local area constant. This may be because there is no axisymmetric shape that fits into the tube and keeps the local surface area constant and is in equilibrium with the flow. A similar conclusion is reached by Leyrat-Maurin *et al.* (1995) in the case of an hyperbolic pore.

In their study of closely fitting area-incompressible capsules, Halpern & Secomb (1989) first neglect the membrane shear resistance (this corresponds to large values of ε). They then determine the steady shape of capsules with different sphericity index flowing in tubes with radius slightly larger than the corresponding critical radius (their figure 9). They also find steady-state shapes when shear and bending resistance are included, assuming that the unstressed reference shape of the membrane is spherical.

Halpern & Secomb did not encounter the same effect of pore plugging as we did. Of course, their reference state for the membrane is either irrelevant (large-ε case) or different from ours, since we considered the initial spheroid as being the unstressed reference state. However the main difference between the two studies is that their sphericity index (from 0.72 to 0.82) is much smaller than ours (0.97). It is then quite
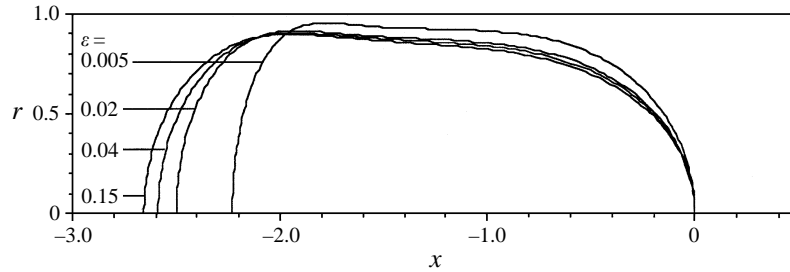
FIGURE 24. Effect of capillary number ε on the steady shape of a spheroidal capsule with $R = 1.2$, $D = 0.8$ and with maximum area change of 1.5% . The numbers indicate the corresponding values of ε.
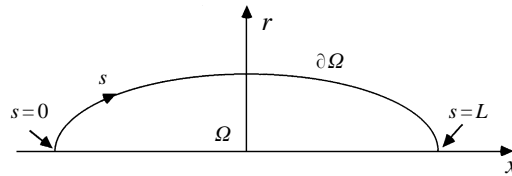

FIGURE 25. Schematics of domain Ω.

possible that the flow of a capsule in a tube is influenced in a complicated way by sphericity index, size ratio and membrane constitutive equation. This point would be interesting to investigate more fully.

When a small area dilatation is allowed, a steady solution can be found. For example, the steady profiles obtained for different values of ε and for a maximum surface area change of about 1.5% are shown on figure 24. The capsule tends to form a slug and thus undergoes a drastic shape change from oblate to prolate. The back of the particle is not concave, as it is for a neo-Hookean capsule. The largest area dilatation occurs at the front of the particle. These shapes are quite similar to those obtained by Halpern & Secomb. The corresponding steady pressure drop evolution is shown on figure 22. The pressure drop becomes insensitive to ε for strong flows and no tendency towards burst is observed.

Appendix

Consider a closed axisymmetric domain Ω bounded by surface $\partial\Omega$ (figure 25). The cylindrical coordinates (r, θ, x) of points on $\partial\Omega$ may be defined in terms of the arclength s of a meridian curve:

$$x = x(s) \quad \text{and} \quad r = r(s),$$

with $r(0) = r(L) = 0$, where x is the revolution axis, s is oriented in the same direction as x, and L is the length of a meridian curve. Then, the surface area $A(s)$ of $\partial\Omega$, measured from the point where $s = 0$, is given by

$$A(s) = \int_0^s 2\pi\, r(u)\mathrm{d}u,$$

and is a monotonic increasing function of s, since r is non-negative. The total surface area A_T of $\partial\Omega$ is then simply

$$A_T = A(L).$$

Consider now another axisymmetric domain Ω' bounded by $\partial\Omega'$, with same total surface area A_T. The points of $\partial\Omega'$ are defined by the arclength s' along a meridian curve, so that the surface area measured from the point where $s' = 0$ is also given by

$$A'(s') = \int_0^{s'} 2\pi\, r'(u')\mathrm{d}u' \quad \text{with} \quad A_T = A'(L').$$

Since $A(s)$ and $A'(s')$ are monotonic functions, there exists a unique mapping of $\partial\Omega$ onto $\partial\Omega'$ that conserves locally the surface area and that is given by

$$s = A^{-1}[A'(s')].$$

This mapping is independent of the volume V (or V') of Ω (or Ω'), which is given by

$$V = \int_0^L \pi r^2\,(s)\,\mathrm{d}x(s),$$

and leads to an integral equation for the function $x(s)$.

This proof has been pointed out by Professor R. Skalak.

REFERENCES

BARTHÈS-BIESEL, D. 1991 Role of interface properties on the motion and deformation of capsules in shear flow. *Physica* A **172**, 103–124.

BARTHÈS-BIESEL, D. & RALLISON, J. M. 1981 Time dependent deformation of a capsule freely suspended in linear shear flow. *J. Fluid Mech.* **113**, 251–267.

BURGER, A. & REHAGE, H. 1992 From two-dimensional model networks to microcapsules. *Ang. Makromol. Chem.* **202-203**, 31–44.

CHANG, K. S. & OLBRICHT, W. L. 1993*a* Experimental studies of the deformation of a synthetic capsule in extensional flow. *J. Fluid Mech.* **250**, 587–608.

CHANG, K. S. & OLBRICHT, W. L. 1993*b* Experimental studies of the deformation and break-up of a synthetic capsule in steady and unsteady simple shear flow. *J. Fluid Mech.* **250**, 609–633.

DROCHON, A., BARTHÈS-BIESEL, D., BUCHERER, C., LACOMBE, C. & LELIEVRE, J. C. 1993 Viscous filtration of red blood cell suspensions. *Biorheology* **30**, 1–8.

FISCHER, T. M., STOHR, M. & SCHMID-SCHÖNBEIN, H. 1978 Red blood cell microrheology: comparison of the behaviour of single RBC and liquid droplets in shear flow. *AIChE Symp. Ser.* **74**, 34–45.

FISHER, T. C., WENBY, R. B. & MEISELMAN, H. J. 1992 Pulse shape analysis of red blood cell micropore flow via new software for the cell transit analyser. *Biorheology,* **29**, 185–201.

GREEN, A. E. & ADKINS, J. C. 1960 *Large Elastic Deformation and Non-linear Continuum Mechanics.* Oxford University Press.

HALPERN, D. & SECOMB, T. W. 1989 The squeezing of red blood cells through capillaries with near minimal diameters. *J. Fluid Mech.* **203**, 381–400.

HSU, R. & SECOMB, T. W. 1989 Motion of non-axisymmetric red blood cells in cylindrical capillaries. *J. Biomech. Engng* **111**, 147–151.

HYMAN, W. A. & SKALAK, R. 1972 Viscous flow of liquid drops in a cylindrical tube. *Appl. Sci. Res.* **26**, 27–52.

KELLER, S. R. & SKALAK, R. 1982 Motion of a tank-treading ellipsoidal particle in a shear flow. *J. Fluid Mech.* **120**, 27–47.

LADYZHENSKAYA, O. A. 1969 *The Mathematical Theory of Viscous Incompressible Flow.* Gordon and Breach.

LEYRAT-MAURIN, A. & BARTHÈS-BIESEL, D. 1994 Motion of a spherical capsule through a hyperbolic constriction. *J. Fluid Mech* **279**, 135–163 (referred to herein as I).

LEYRAT-MAURIN, A., DROCHON, A., LEVERGER, A. & BARTHÈS-BIESEL, D. 1995 Effect of geometry and membrane properties on the flow of capsules through a short pore at constant pressure drop. *Biorheology* **32** 312–313.

LI, X. Z., BARTHÈS-BIESEL, D. & HELMY, A. 1988 Large deformations and burst of a capsule freely suspended in an elongational flow. *J. Fluid Mech.* **187**, 179–196.

LONGUET-HIGGINS, M. S. & COKELET, E. D. 1976 The deformation of steep surface waves on water I. A numerical method of computation. *Proc. R. Soc. Lond.* A **350**, 1–26.

MARTINEZ, M. J. & UDELL, K. S. 1990 Axisymmetric creeping motion of drops through circular tubes. *J. Fluid Mech.* **210**, 565–591.

OLBRICHT, W. L. & KUNG, D. M. 1992 The deformation and break-up of liquid drops in low Reynolds number flow through a capillary. *Phys. Fluids* A **7**, 1347–1354.

POZRIKIDIS, C. 1990 The axisymmetric deformation of a red blood cell in uniaxial straining Stokes flow. *J. Fluid Mech.* **216**, 231–254.

POZRIKIDIS, C. 1992 *Boundary Integral and Singularity Methods for Linearized Viscous Flow.* Cambridge University Press.

POZRIKIDIS, C. 1995 Finite deformation of liquid capsules enclosed by elastic membranes in simple shear flow. *J. Fluid Mech.* **297**, 123–152.

QUÉGUINER, C. 1995 Modélisation de l'écoulement d'une capsule dans un pore cylindrique. Thesis. Doctorat de l'Université de Technologie de Compiègne.

RALLISON, J. M. & ACRIVOS, A. 1978 A numerical study of the deformation and burst of a viscous drop in an extensional flow. *J. Fluid Mech.* **89**, 191–200.

SECOMB, T. W. 1995 Mechanics of blood flow in the microcirculation. In *Biological Fluid Dynamics,* (ed. C. P. Ellington & T. J.Pedley), pp. 305–321 Company of Biologists, Cambridge.

SECOMB, T. W. & HSU, R. 1995 Red blood cell mechanics and functional dcapillary density. *Intl J. Microcirc.* **15**, 250–254.

SECOMB, T. W., SKALAK, R., ÖZKAYA, N. & GROSS, J. F. 1986 Flow of axisymmetric red blood cells in narrow capillaries. *J. Fluid Mech.* **163**, 405–423.

SKALAK, R., TOZEREN, A., ZARDA, R. P. & CHIEN, S. 1973 Strain energy function of red blood cell membranes. *Biophys. J.* **13**, 245–264.

SKALAK, R., ÖZKAYA, N. & SKALAK, T. C. 1989 Biofluid mechanics. *Ann. Rev. Fluid Mech.* **21**, 167–204.

STONE, H. A. 1994 Dynamics of drop deformation and break-up in viscous fluids. *Ann. Rev. Fluid Mech.* **26**, 65–102.

SUTERA, S. P., PIERRE, P. R. & ZAHALAK, G. I. 1989 Deduction of intrinsic mechanical properties of the erythrocyte membrane from observations of tank-treading in the rheoscope. *Biorheology* **26**, 177–197.

SUTERA, S. P., SESHADRI, V., CROCE, P. A. & HOCHMUTH, R. M. 1970 Capillary blood flow II. Deformable model cells in tube flow. *Microvasc. Res.* **24**, 296–313.

YOUNGREN, G. K. & ACRIVOS, A. 1975 Stokes flow past a particle of arbitrary shape: a numerical method of solution. *J. Fluid Mech.* **69**, 377–403.

ZHOU, H. & POZRIKIDIS, C. 1995 Deformation of liquid capsules with incompressible interfaces in simple shear flow. *J. Fluid Mech.* **283**, 175–200.